Applied Geochemistry 27 (2012) 44–55

Contents lists available at SciVerse ScienceDirect

Applied Geochemistry

journal homepage: www.elsevier.com/locate/apgeochem

Deciphering interaction of regional aquifers in Southern Tunisia using hydrochemistry and isotopic tools

Kamel Abid [a,*], Marek Dulinski [b], Friha Hadj Ammar [a], Kazimierz Rozanski [b], Kamel Zouari [a]

[a] École Nationale d'Ingénieurs de Sfax, BP: W 3038 Sfax, Tunisia
[b] AGH University of Science and Technology, Faculty of Physics and Applied Computer Science, al. Mickiewicza 30, 30-059 Krakow, Poland

ARTICLE INFO

Article history:
Received 28 January 2011
Accepted 29 August 2011
Available online 7 September 2011
Editorial handling by W.M. Edmunds

ABSTRACT

Groundwater is the most important source of water supply in southern Tunisia. Previous hydrogeologic and isotopic studies carried out in this region revealed the existence of two major aquifer systems: the "Complex Terminal" (CT) and the "Continental Intercalaire" (CI). Turonian carbonates constitute one of the major aquifer levels of the CT multilayered aquifer. It extends over most of southern Tunisia, and its hydrodynamic regime is largely influenced by tectonics, lithology and recharge conditions. Forty-eight groundwater samples from the CI and Turonian aquifers were collected between January and April 2004 for chemical and isotopic analyses. Hydrochemistry and isotopic tools were combined to get an insight into the processes controlling chemical composition of groundwater and wide-scale interaction of these two aquifer systems. Analysis of the dissolved constituents revealed that several processes control the observed chemical composition: (i) incongruent dissolution of carbonate minerals, (ii) dissolution of evaporitic minerals, and (iii) cation exchange. Dissolution alone cannot account for the observed high supersaturation states of groundwater with respect to calcite and dolomite. The observed supersaturation is most probably linked to geogenic CO_2 entering water-bearing horizons of the CT and CI aquifers via deep tectonic faults and discontinuities and subsequent degassing in the exploitation wells. Presence of geogenic CO_2 in the investigated region was confirmed by C isotope data of the DIC reservoir. The radiocarbon content of the Turonian samples varied between 9.5 and 43 pmc. For CI samples generally lower values were recorded, between 3.8 and 22.5 pmc. Stable isotope composition of Turonian groundwater samples varied from −8.3 to −5.3‰ for $\delta^{18}O$ and from −60 to −25‰ for $\delta^{2}H$. The corresponding ranges of δ values for the Continental Intercalaire samples were from −8.9‰ to −6.9‰ for $\delta^{18}O$ and from −68.2‰ to −45.7‰ for $\delta^{2}H$. Stable isotope composition of groundwater representing CT and CI aquifers provide strong evidence for regional interaction between both systems.

© 2011 Elsevier Ltd. All rights reserved.

1. Introduction

Studies of the origin of groundwater and processes leading to its mineralization are important for proper evaluation and management of water resources, especially in arid and semi-arid regions. In these regions, general scarcity and poor quality of surface water often results in intensive exploitation of groundwater resources, without taking into account its potential vulnerability to over-exploitation and pollution from the surface. As a consequence, gradual lowering of water table and degradation of water quality is a wide-spread phenomenon in those regions, causing serious problems for local users. To ensure the long-term sustainability of groundwater resources, managers need to have detailed information on the exploited groundwater systems. The integration of hydrochemical and isotopic tools play a very important role here, allowing better understanding of recharge processes, groundwater dynamics and water–rock interaction in a variety of climates and geological settings (e.g. Clark and Fritz, 1997; Edmunds et al., 2003).

Tunisia suffers from limited surface water resources, particularly in its southern part. Consequently, numbers of studies have been carried out in the past decades (ERESS, 1972; Gonfiantini et al., 1974; Edmunds et al., 1997, 2003; OSS, 2003) with the main aim of evaluating the potential of groundwater resources in this region. Two major aquifer systems have been identified in southern Tunisia: (i) the "Continental Intercalaire" (CI) logged in the continental formations of the lower Cretaceous, and (ii) the "Complex Terminal" (CT) hosted in carbonate formations of the Turonian and Senonian as well as in sandstone formations of the Mio-Pliocene. These large, regional aquifer systems are shared between Algeria, Tunisia and Libya. Nowadays, more than 600 boreholes exploit water from different aquifer levels with the mean productivity equal to approximately 170 $Mm^3\,a^{-1}$ (OSS, 2003). Previous hydrogeological investigations have proved the existence of

* Corresponding author. Tel./fax: +216 74275595.
E-mail address: kamel_hydrology@hotmail.com (K. Abid).

0883-2927/$ - see front matter © 2011 Elsevier Ltd. All rights reserved.
doi:10.1016/j.apgeochem.2011.08.015

hydraulic connections between different levels of the CI and CT aquifers through the existing faults (Mamou, 1990; Edmunds et al., 1997; OSS, 2003; Kamel, 2007). However, possible links between the Turonian formation and the CI aquifer have never been investigated.

The principal aim of the present study was to integrate hydrochemistry and isotopic tools in order to shed light on the origin and chemical evolution of groundwater in the Turonian formation and to investigate a possible contribution of water from the deep CI aquifer to this formation, thus aiding sustainable use of these groundwater resources. Both studied aquifers are considered a major strategic reserve of potable and irrigation water in southern Tunisia.

2. Study area

Southern Tunisia (7°30′E –10°30′E, 30°10′N –34°10′N) extents to the Algerian border in the west and to the Djeffara plain of the Gabes and Dahar mountains in the east. In the north, it is limited by the Chotts region and in the south by the Saharan platform (Fig. 1). The region is characterized by an arid climate with the mean annual precipitation not exceeding 100 mm. The mean annual temperature is about 21 °C, while potential evapotranspiration exceeds 1700 mm a^{-1} (Kamel, 2007).

2.1. Geology and hydrogeology

The regional geology of southern Tunisia has been discussed by several authors (e.g. Busson, 1967; Bouaziz, 1995) and only its essential aspects relevant to the present work are recalled here. Geophysical investigations and boreholes completed recently in the region have allowed a more detailed understanding of the hydrogeology of southern Tunisia.

The study area consists of up-lifts and subsiding basins whose geologic formations show substantial variability, both in lithology and thickness. This structure is the result of different tectonic events. The characteristic feature of the study area is the NW–SE anticline developed through major compressive movement during the Lower Pliocene (Atlas Phase). Four different structural units can be distinguished in the investigated area (Fig. 1).

2.1.1. The Saharan platform

This extends from the Dahar upland to the Algerian border. Mio-Pliocene sands and Turonian and Senonian limestones are

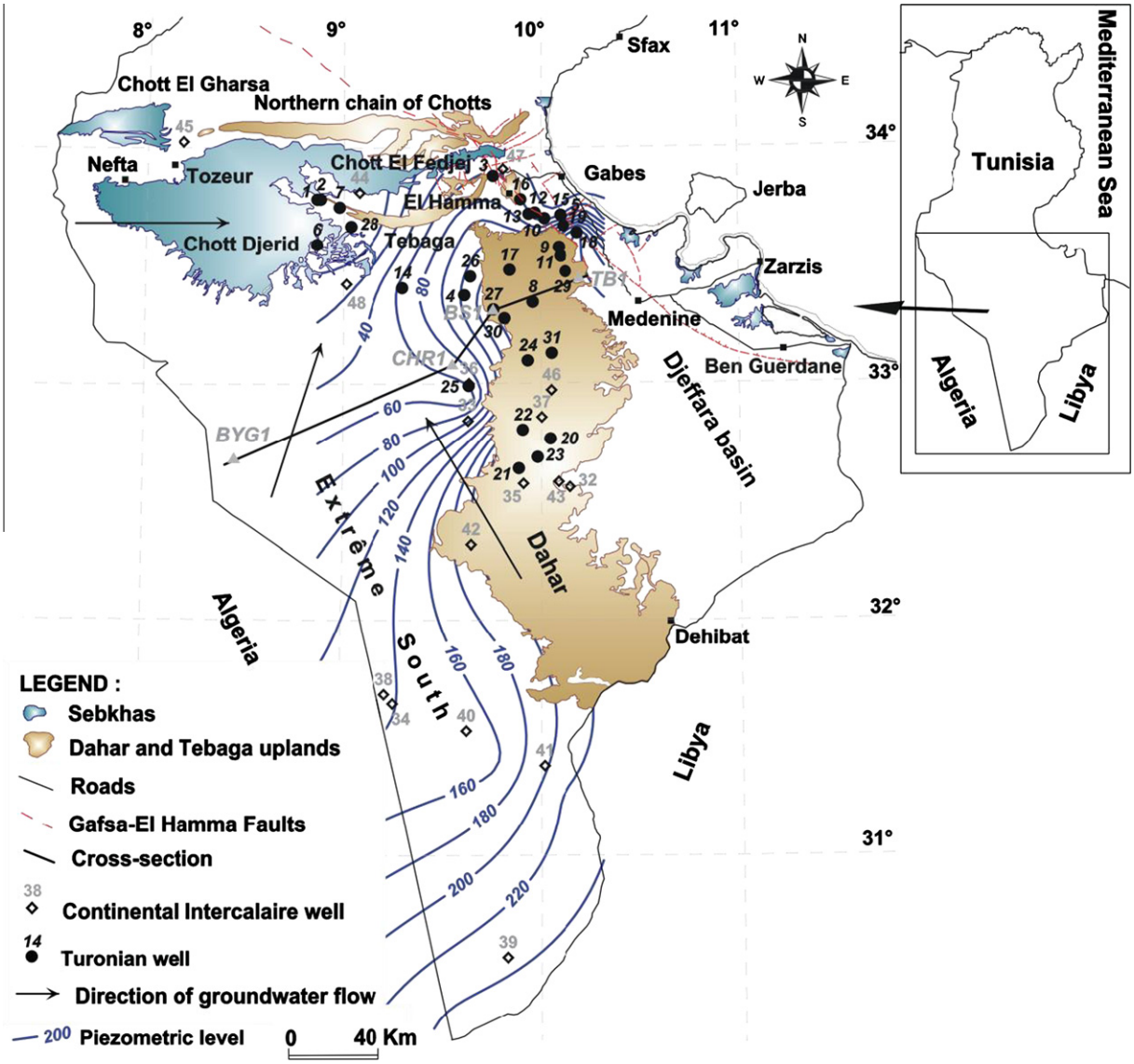

Fig. 1. Schematic map of the study area. Sampled wells are marked by numbers. Cross-section shown in Fig. 2 is marked by heavy line.

present all over this area. Their thickness exceeds 500 m. The Turonian carbonates are lithologically homogenous in this part of the basin and outcrop on surrounding uplands due to the presence of several N–S and W–E faults. South of 32°30′N the Turonian and Senonian carbonate aquifers are not exploited.

2.1.2. The Dahar upland

This unit in its eastern part is bounded by a set of faults generated during the Late Cretaceous (Coniacian–Santonian) extensional event (Boltenhagen, 1981; Ellouze, 1984; Bouaziz et al., 2002). Marls and Senonian limestones overlie the Turonian carbonates and outcrop in this part of the basin. In the northern part of the Dahar upland, these formations overlie the Jurassic bedrocks. The Turonian aquifer is exploited in the central and northern part of the Dahar upland.

2.1.3. The Chotts region

The Mio-Pliocene sands, carbonate and lacustrine Senonian deposits and Turonian carbonates are the main formations in this area. The Middle and Upper Turonian aquifer is formed here by an alternation of limestones, shale, gypsum and fossiliferous marls (Bouaziz, 1995).

2.1.4. The Djeffara basin

The basin is located in the eastern part of the study area. The region adjacent to Gulf of Gabes is recognised as the discharge area of the CI and CT aquifers with an overall evaporative discharge in the order of 0.3 $m^3 s^{-1}$ (ERESS, 1972). The thickness of Turonian carbonates varies spatially (Abidi and Ben Baccar, 2001; OSS, 2003). In the south-eastern part of the basin (Djeffara of Medenine and Tataouine) Turonian carbonates are missing. These stratigraphic gaps are due to several factors such as irregularity of the paleotopography, eustatic movements and tectonic instabilities (Castany, 1954; Ellouze, 1984; Bouaziz,1995).

The main directions of groundwater flow are from Algeria (W–E and SW–NE) as well as from the Dahar region of Tunisia. Most of recharge occurs at outcrops around the Dahar uplands in the SE, and from the northern chain of the Chotts in the north (Abid, 2010; Abid et al., 2011). Discharge from the aquifer occurs through wells, natural springs and vertical percolation at the sabkha surfaces (OSS, 2003). Seismic profiles and lithostratigraphic correlations show that the Turonian aquifer is affected by major faults which are likely to generate some lateral compartmentalization leading to complexity of groundwater flow.

Geological formations that host the CI aquifer show significant lateral variation in facies and in thickness, when one moves out from the Saharan platform towards the Chotts region. Changes in sedimentation within the fluvio-deltaic continental deposits produced a complex succession of detrital levels with clayey horizons and frequent gypsum intercalations (Bouaziz, 1995; Edmunds et al., 2003). However, the aquifer is hydraulically continuous over the whole basin.

A representative SW–NE cross-section of the investigated area is shown in Fig. 2. Sedimentary formations are displayed in a 20–30° south-dipping monocline affected by E–W striking faults along the northern edge of the Dahar upland (Gabtni et al., 2009). This structure seems to have controlled the formation of the Upper Cretaceous deposits and plays a major role in the groundwater flow. In the study area, the Turonian carbonates outcrop in the Tebaga and the Dahar uplands owing to the presence of several N–S and W–E faults. Their thickness varies from 20 to 85 m, but in some parts of the area it exceeds 100 m. The presence of marls in the Turonian deposits appears to be very irregular. Marls and limestones of the Senonian overlie the Turonian deposits and outcrop in the Dahar upland.

3. Materials and methods

Groundwater samples were collected between January and April 2004. Altogether, 31 samples from the Turonian and 17 samples from the CI aquifer have been collected. The location of the sampled wells is shown in Fig. 1. Several parameters such as pH, electrical conductivity (EC), temperature and alkalinity (HCO_3) were measured on-site for each well. Samples for analyses of major ions were filtered (0.45 mm, paper filter) and collected in plastic bottles and analyzed within a few days. Precipitation of $BaCO_3$ for ^{14}C and ^{13}C analysis was done in the field using the method described by Haynes and Haas (1980). Unfiltered groundwater samples were collected in 30 mL polyethylene bottles with poly-seal caps for stable isotope analysis.

The analyses of major ions were performed at the Laboratory of Radio-Analyses and Environment of the National Engineering School of Sfax (ENIS, Tunisia). The results were tested for charge balance (Freeze and Cherry, 1979). The calculated charge balance errors were generally less than ±5%, which was considered an acceptable level for the purpose of this study. The detection limit was approximately 0.05 mg L^{-1} for all analyzed elements.

Stable isotope ratios of water ($^{18}O/^{16}O$ and $^{2}H/^{1}H$) were determined at the laboratory of the International Atomic Energy Agency (IAEA) in Vienna using the standard CO_2 equilibration method (Epstein and Mayeda, 1953) and reduction of water on metallic Zn (Coleman et al., 1982), respectively. Analyses are reported in the δ notation representing ‰ deviations from the VSMOW standard (Vienna-Standard Mean Oceanic Water) on a scale such that $\delta^{18}O$ and $\delta^{2}H$ of Standard Light Antarctic Precipitation (SLAP) is −55.5‰ and 428‰, respectively (Coplen, 1996). Analytical uncertainty was equal ±0.1‰ for $\delta^{18}O$ and ±1.0‰ for $\delta^{2}H$ analyses.

Radiocarbon content in the precipitated $BaCO_3$ samples was determined at the Laboratory of Radio-Analyses and Environment of the National Engineering School of Sfax (ENIS, Tunisia) using benzene synthesis and liquid scintillation spectrometry. The $^{13}C/^{12}C$ ratios were determined by isotope ratio mass spectrometry at the IAEA laboratory. The $^{13}C/^{12}C$ ratios are reported as δ values expressed relative to VPDB on a scale such that NBS-19 calcite is −2.2‰. Radiocarbon concentrations are reported as percent of modern carbon (pmc) (Stuiver and Polach, 1977). Uncertainties are equal ±1 pmc and ±0.3‰ for ^{14}C and ^{13}C measurements, respectively.

4. Results and discussion

4.1. Hydrochemistry

Results of chemical and isotope analyses of water samples from the Turonian and CI aquifer are presented in Table 1. Mineralization of groundwater varied from 542 to 8029 mg L^{-1} and from 1620 to 6090 mg L^{-1}, for CT and CI aquifers, respectively. Temperature of Turonian water samples varied from 16.1 to 31 °C. Lower water temperature was recorded in the vicinity of Cretaceous and Miocene outcrops (recharge areas), whereas higher values were measured in the tectonic zones of the Gabes and Chott el Fedjej regions. Generally higher temperatures were observed in the CI aquifer (range from 20 °C to 69 °C, with the exception of well No. 46). Temperatures of water and filter depths are not well correlated probably due to the influence of air temperature on the shallow wells and/or leakage of water from deeper aquifer levels. Indeed, highest water temperatures in the CT aquifer were observed in the vicinity of the El Hamma Faults (Gourai: 31 °C; El Hamma Mzirâa: 29.5 °C), pointing to upward leakage of the CI aquifer in this area.

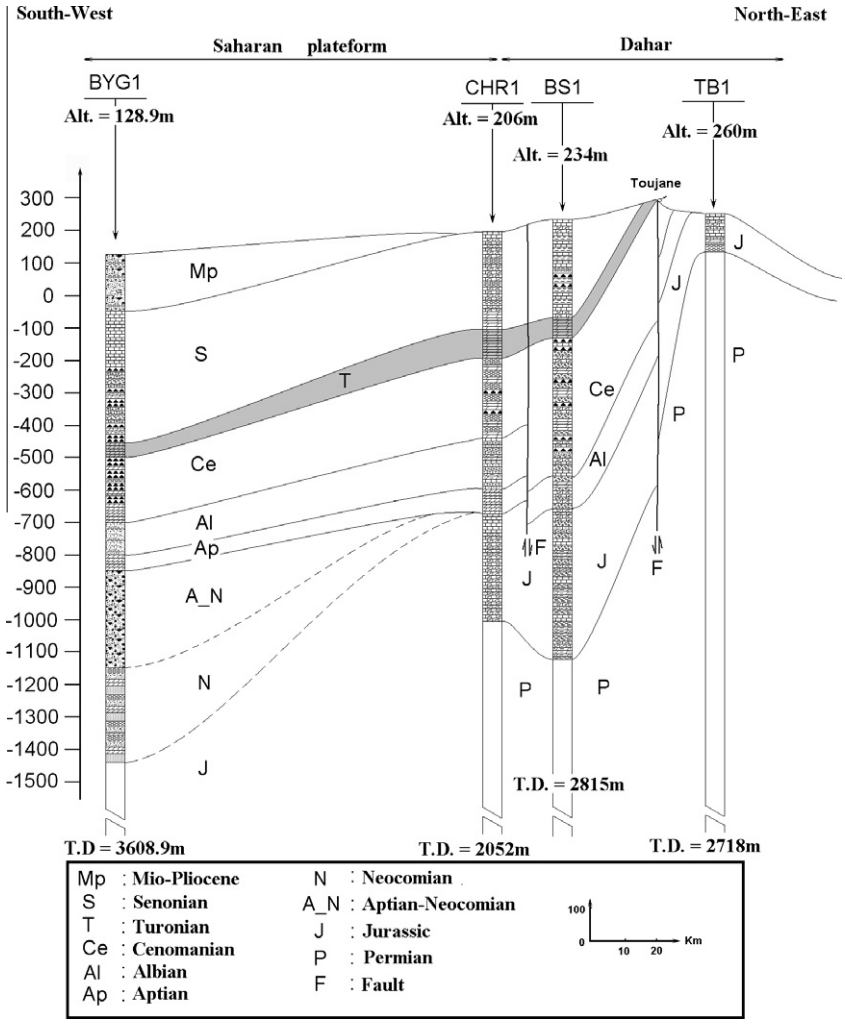

Fig. 2. Hydrogeological cross section in the study area.

Two groups of groundwater can be distinguished in the Turonian aquifer on the basis of major ion content (Fig. 3). The first group of "SO_4–Cl–Ca to mixed" waters includes wells located in the vicinity of the El Hamma sill and tectonic zones of the Gabes and Chott el Fedjej regions. It is characterized by lower concentration of Na and HCO_3 ions, coupled with higher concentration of SO_4. The presence of mixed-water type reflects the influence of water from the CI aquifer ascending to the Turonian through systems of deep faults. The second group of weakly mineralized waters (SO_4–Na to mixed) is represented by wells located in the vicinity of outcrops (Dahar upland). This groundwater is draining gypsiferous and halite deposits and its mineralization is dominated by Na and SO_4 ions.

Principal component analysis (PCA) has been applied to determine the relationship between ionic constituents measured in the CI and CT aquifers and the geological setting (Esbensen, 2002). Properties of groundwater were described by eight variables (Fig. 4) representing major ion concentrations (Cl^-, Na^+, SO_4^{2-}, Ca^{2+}, Mg^{2+}, K^+ and HCO_3^-) and total mineralization (TDS) measured in the laboratory.

The two principal axes of PCA explain 61% of the sampling variance. This percentage is relatively low, indicating dependence of the chemical composition of analyzed waters on a number of factors. The negative part of PC1 axis represents the content factor determined by Cl^-, Na^+ and K^+, whereas Mg^{2+}, Ca^{2+} and SO_4^{2-} concentrations determine its positive part (Fig. 4a). This axis reflects the role of dissolution of evaporite minerals (halite, gypsum, and/or anhydrite) of the observed mineralization. The location of the majority of waters originating from the CI aquifer in the negative part of the PC1 axis shows that increase of salinity is essentially forced by dissolution of halite (Fig. 4b). This is in agreement with the distribution of data points on the Piper diagram showing that anionic mineralization of CI groundwater is dominated by Cl^- content. A cluster of points in the positive part of the PC1 axis represents mostly groundwater from the Turonian aquifer in which the SO_4^{2-} ion is dominant. Moreover, the opposing location of Na^+ with respect to Ca^{2+} and Mg^{2+} cations (Fig. 4a) confirms to some extent the $(Ca^{2+} + Mg^{2+})/Na^+$ cation exchange. The PC2 axis describes mainly TDS and HCO_3^- concentrations. Both axes reflect also the spatial origin of mineralization. The lowest values of TDS are recorded in wells 23, 8, 17 and 29 located in the Dahar upland (Fig. 4b).

Based on Fig. 4, two groups of waters can be distinguished: (i) waters from the Dahar upland, characterized by the lowest mineralization, Mg^{2+} and alkalinity content, which may reflect the relatively short residence time of groundwater, indicating the presence of a young, local component which probably enters the system via faults and/or fractures, (ii) waters from the tectonic zones of the Gabes and Chott el Fedjej regions having the highest mineralization, Mg^{2+} and alkalinity content acquired during slow

Table 1
Isotopic and geochemical data for Turonian and CI aquifers.

Aquifer	Well No.	Name	Elevation (m)	Filter depth (m)	EC (μS cm^{-1})	T (°C)	pH	Na^+ (mg L^{-1})	Ca^{2+} (mg L^{-1})	Mg^{2+} (mg L^{-1})	K^+ (mg L^{-1})	Cl^- (mg L^{-1})	SO_4^{2-} (mg L^{-1})	TDS (mg L^{-1})	HCO_3^- (mg L^{-1})	$\delta^{18}O$ (‰)	δ^2H (‰)	$\delta^{13}C$ (‰)	^{14}C (pmc)
Turonian	1	Ziret Louhichi	36	75	4790	24.7	7.6	516.0	406.0	136.5	<0.05	741.0	1595.9	3770	134.2	−6.72	−48.5		
	2	Ziret Ouled Touati	37	44	4830	25.3	7.3	545.9	438.2	144.6	<0.05	829.5	1704.0	3880	146.4	−6.80	−47.5	−4.5	11.2
	3	El Hamma Mziraa	63	342	4490	29.5	7.9	588.3	332.4	82.4	<0.05	859.6	1131.8	3240	36.6	−8.31	−57.8		
	4	Zoumit	199	355	3560	26.7	7.4	387.8	284.7	111.9	<0.05	559.2	1152.7	2730	134.2	−7.24	−54.0	−7.3	30.2
	5	Garet Ltaifa	101	233	3480	23.3	7.2	370.0	274.5	102.6	<0.05	500.2	1129.3	2640	115.9	−6.97	−49.3	−6.2	12.5
	6	Oum Laabid	27		3480	20.5	8.1	352.6	229.4	175.8	<0.05	321.2	1650.8	2940	18.3	−7.50	−56.0		
	7	Oued El Melah	55		3200	21.6	7.6	216.3	421.4	100.5	<0.05	204.1	1556.5	2910	109.8	−5.25	−25.2		
	8	Zmerten	361		1150	27.2	7.5	234.9	99.4	44.1	<0.05	204.0	402.2	700	225.7	−6.70	−39.1	−8.1	11.4
	9	Beni Zelten Sonède	220	150	2610	22.7	7.2	243.1	257.2	110.1	<0.05	400.5	891.5	2040	183.0	−5.80	−31.9	−6.6	37.0
	10	Matmata 5	125	375	4690	20.2	7.5	550.4	382.6	157.8	<0.05	939.9	1402.2	3750	122.0	−6.92	−49.7	−5.2	11.4
	11	Beni Zelten 3	210	50	3450	23.7	7.2	268.1	382.6	119.6	<0.05	376.6	1386.1	2820	176.9	−6.05	−32.5	−7.8	43.0
	12	Henchir Jehha	113	410	3740	25.0	7.6	394.3	302.9	111.1	<0.05	567.2	1263.0	2870	122.0	−7.01	−51.6	−6.5	9.5
	13	Matmata Aéreport	135	515	3750	24.8	7.5	408.3	300.5	105.1	<0.05	584.3	1154.2	2890	122.0	−7.34	−52.2		
	14	Tinia	85	670	8940	24.4	7.8	1165.4	601.1	254.7	<0.05	2057.2	2329.9	7020	24.4	−7.74	−53.7		
	15	Lymaoua5	68	140	3900	27.0	7.6	357.7	301.7	85.2	10.7	484.2	1023.6	2622	36.6	−6.55	−46.2		
	16	Gourai	107	550	4060	31.0	7.5	397.1	388.2	87.4	16.0	547.1	1131.3	3134	134.2	−7.34	−52.2	−5.5	11.0
	17	Merbah Sandoug	295	350	1680	27.6	7.8	240.7	222.5	66.0	<0.05	271.9	684.2	1200	164.7	−6.73	−42.6	−7.0	18.1
	18	Pepiniere Tounine	225	70	9650	20.0	8.0	884.7	842.6	353.0	89.5	1995.7	2455.1	8029	152.5	−6.03	−36.6		
	19	Zaten	224	109	1730	22.0	7.8	253.0	54.0	66.0	9.0	298.0	365.0	1080	66.0	−5.49	−32.8		
	20	Echahba	380		4810	16.1	7.6	550.8	521.5	208.0	81.0	920.8	2153.2	3739	115.9	−8.13	−59.0		
	21	Sih Essraya	350		4350	22.4	8.3	417.8	233.2	131.2	45.3	1065.8	541.8	3134	24.4	−8.04	−60.1		
	22	Guelb Eddoukhane	330		4830	22.8	8.3	414.5	303.6	101.8	65.5	655.1	1385.8	3677	12.2	−7.85	−55.1		
	23	Bir Echahba	360		500	21.6	7.2	141.4	100.7	57.7	15.5	144.2	407.9	967	213.5	−6.23	−37.5		
	24	Zridib	271		2300	22.7	8.1	640.1	221.8	110.6	<0.05	639.6	1108.3	2900	170.8	−6.81	−46.9	−6.7	16.9
	25	Bou Flija	190	207	5600	28.0	7.7	740.3	296.6	139.8	24.6	1443.1	745.1	4222	158.6				
	26	Bel Habel		219	3290	22.0	7.5	328.0	256.0	205.0	9.0	568.0	1276.0	2600	75.0				
	27	Bir Soltane	250	325	3486	22.0	7.2	375.0	288.0	95.0	<0.05	461.0	1066.0	2440	146.0				
	28	Bazma Turonien			6400	22.0	7.9	542.6	669.3	243.2	24.6	815.5	2304.0	5452	244.0				
	29	Source Toujane			970	20.5	8.4	75.8	70.2	23.9	3.2	119.1	108.4	542	213.5				
	30	El Mthinin	252		3120	22.0	7.8	369.6	256.7	98.0	53.6	528.8	882.4	2452	128.1				
	31	Bel Khchab2	331		2200	22.0	7.8	251.7	128.0	69.3	32.8	437.1	472.5	1500	152.5				
Continental Intercalaire	32	Daghsen 6	390	86	2520	25.2	7.0	345.5	142.6	50.7	13.3	396.7	591.0	1620	140.3	−6.91	−45.7		
	33	Mahbes		620	4710	32.9	8.0	612.0	336.0	137.0	43.0	1140.0	974.0	3252	154.0	−7.70	−57.0	−9.9	5.0
	34	El Borma Henchir	245		6870	34.8	7.5	1096.6	307.6	70.2	<0.05	1565.7	999.2	4510	115.9	−8.78	−66.8	−10.0	16.5
	35	Oued Lisseri	385		4360	20.0	7.5	520.3	234.8	116.5	<0.05	1044.4	858.5	3050	73.2	−8.10	−62.7		
	36	Ksar Ghilane	285	625	6360	34.0	7.6	849.3	483.8	171.9	<0.05	1417.7	1561.0	4860	115.9	−7.01	−49.7		
	37	El Angoud	362		5660	20.6	8.1	693.6	394.4	163.0	<0.05	1236.5	1356.8	4190	140.3	−7.02	−46.9		
	38	El Borma A8	271		4800	33.6	7.8	1180.7	293.4	74.0	<0.05	1492.2	1070.6	4360	91.5	−8.92	−68.2		

39	Garaet Tebour5	353		2570	51.0	8.1	370.0	134.0	40.0	43.0	554.0	437.0	1680	198.0	−7.94	−61.1				
40	Larich	272		7550	26.8	7.4	1144.7	549.0	137.6	<0.05	2046.7	1133.7	5240	91.5	−8.56	−66.1	−10.5	3.8		
41	Oued Zar	402		8570	31.5	7.4	1104.4	688.0	184.5	<0.05	2515.6	1009.6	6090	109.8	−8.43	−64.3	−10.7	5.1		
42	Khchem Mariem	300	405	6042	25.0	7.2	726.2	542.2	186.6	<0.05	1707.6	803.6	4230	108.8	−8.34	−64.1				
43	Daghsen 7	393	80	2650	23.6	7.6	292.7	174.3	40.9	18.8	414.8	552.9	1900	140.3	−7.04	−47.2	−7.6	22.5		
44	EL Bahair Cl 9	53	1268	3460	65.0	7.2	363.0	306.0	74.1	46.9	676.0	808.0	2421	128.0	−8.10	−59.0				
45	Hamma Cl 4	75	1368	3510	69.0	8.2	539.6	201.1	23.7	73.4	294.4	1227.4	2860	103.7	−6.99	−48.5				
46	Guelb Fguira	369	94	3100	15.0	8.0	394.1	217.6	29.7	<0.05	431.9	712.1	2180	91.5	−7.23	−49.6	−7.8	10.9		
47	El Hamma Sud Cl	83	1188	5250	50.0		586.4	511.0	60.9	28.1	974.8	1339.5	4029	97.6	−7.87	−59.0				
48	Lazala (Douz Cl)	60	1726	5900	51.6	7.6	888.1	446.7	60.2	97.8	1623.6	913.1	4105	140.3	−8.16	−62.6				

groundwater movement through fissured or poorly karstified carbonates. This supports the hypothesis of an upward leakage of CI groundwater to the Turonian aquifer through deep faults.

In order to further elucidate the geochemical processes that contribute to mineralization of groundwater in the CT and CI aquifers, the observed chemical composition of collected groundwater samples has been analyzed in more detail. The concentrations of Ca^{2+}, Cl^-, Mg^{2+}, Na^+ and SO_4^{2-} ions generally increase with the increasing total mineralization (TDS). The abundance of carbonate rocks and the erosion rates in the study area suggest that the dissolution of carbonate minerals may potentially add significant amounts of Ca^{2+} and Mg^{2+} to groundwater of the Turonian aquifer. Dissolution of calcite is the most common weathering reaction (Drever, 1988). In such a process each 0.5 mol of Ca^{2+} corresponds to one mole of HCO_3^-. Thus, in terms of equivalence ratio the relationship between Ca^{2+} and HCO_3^- should be represented by a straight line with the slope equal to one. Fig. 5a shows that only wells Nos. 8, 19, 23 and 29 fall near the stoichiometric equilibrium line. Points representing all other groundwater samples are situated far above the line, indicating another origin of Ca^{2+}, possibly from dissolution of gypsum and/or cation exchange reactions.

In mudstones and marls, the dissolution of gypsum is the source of SO_4^{2-} and additional Ca^{2+} ions. The plot of Ca^{2+} vs. SO_4^{2-} (Fig. 5b) shows that most of the analyzed groundwater samples fall below the stoichiometric equilibrium line representing $CaSO_4$ dissolution. This depletion in Ca^{2+} content relative to SO_4^{2-} concentration can be linked to several processes: (i) cation exchange reactions in which Ca^{2+} ions are adsorbed on clay minerals with simultaneous release of Na^+ ions (c.f. Fig. 5c), (ii) incongruent dissolution of dolomite and gypsum with simultaneous precipitation of calcite, and/or (iii) precipitation of carbonates due to outgassing of CO_2 (majority of the analyzed groundwater samples are oversaturated with respect to carbonate minerals). If Na^+ ions are derived from dissolution of evaporative minerals, they should balance Cl^- ion content. The plot of Na^+ vs. Cl^- (Fig. 5d) shows that for the majority of wells Na^+ ions are in slight excess with respect to Cl^-. This excess could be due to cation exchange, as suggested already by the Ca^{2+} vs. SO_4^{2-} plot. A significant deficit of Na is observed in wells Nos. 18, 21 and 25 (cf. Fig. 5c). This might stem from the second type of cation exchange, where Na^+ ions are removed from the solution and are replaced by Ca^{2+}. The dashed line in Fig. 5b shows the expected relationship between Ca^{2+} and SO_4^- ions in solution when incongruent dissolution of dolomite and gypsum with simultaneous precipitation of calcite occurs in the system. It is apparent from Fig. 5b that the majority of data points cluster along this line, providing a strong indication of the occurrence of dedolomitization reactions in the studied aquifers.

Dissolution of evaporites is also confirmed by the saturation indices calculated with the aid of the PHREEQC-2 program (Parkhurst and Appelo, 1999). They show that almost all samples are undersaturated with respect to halite (Fig. 6a) and gypsum (Fig. 6b).

The relationship between saturation indices with respect to calcite (SI_C) and dolomite (SI_D) of groundwater samples representing CT and CI aquifers is presented in Fig. 7. The saturation indices cover the range between −0.4 and 1.1 for calcite and from −0.9 to 2.15 for dolomite. The data points are distributed along the straight line $SI_D = 1.85,\cdot SI_C - 0.07$ ($R = 0.975$, $N = 47$). Most of the analyzed waters are supersaturated with respect to both carbonate minerals.

Outgassing of CO_2 is the primary process responsible for supersaturation of the studied groundwaters with respect to carbonate minerals. This process was modeled with the aid of the PHREEQC-2 code. The calculations were performed assuming the concept of open or closed systems with respect to gaseous CO_2. The central assumption in the open-system model is that infiltrating water is in permanent contact with an infinite reservoir of CO_2

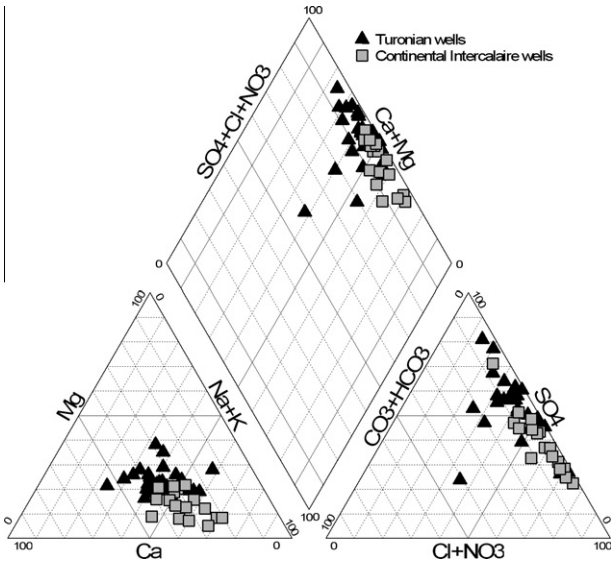

Fig. 3. Piper diagram of Turonian and Continental Intercalaire groundwater samples.

and the solid phase being dissolved until saturation conditions are reached. Under closed-system conditions, water initially equilibrates with CO_2 but is allowed to dissolve the solid phase only after the contact with CO_2 reservoir is terminated. It is believed that these two models represent extreme situations which may occur under natural conditions.

The results of model calculations are presented in Fig. 8. The calculated trend lines for the outgassing process are in satisfactory agreement with the observed pH and SI_C values for pCO_2 equal 0.02 and 0.08 atm, for solutions formed under open- and closed-system conditions, respectively. The later value, in particular, is too high for the recharge areas of the investigated groundwater systems. Thus, to carry on outgassing of CO_2 to the extent required by the observed range of supersaturation states with respect to calcite and dolomite, an additional source of CO_2 of geogenic origin, apart from soil CO_2, would be required in the investigated systems (cf. discussion in Section 4.2). Outgassing processes should lead to precipitation of carbonate minerals, which has been in fact observed in many exploited wells in the study area.

4.2. Carbon isotopes

The $^{13}C/^{12}C$ and $^{14}C/^{12}C$ ratios in the dissolved inorganic C pool (DIC) were measured in 17 out of 48 sampled wells. As seen from Table 1, a relatively wide range of both radiocarbon content and $\delta^{13}C$ values of the DIC reservoir was observed, from 3.8 pmc to 43 pmc for radiocarbon and from −4.5‰ to −10.5‰ for $\delta^{13}C$. The highest measured radiocarbon content (43 pmc) was observed in a relatively shallow well (No. 11) located close to the Gulf of Gabes. In this well also ^{3}H was detected (ca. 1.3 TU) pointing to admixture of fresh water. The lowest value (3.8 pmc) was found in well No. 40 tapping the IC aquifer.

An attempt was made to model the observed range of radiocarbon content and $\delta^{13}C$ values of the DIC pool using the PHREEQC-2 code. The ^{14}C and ^{13}C isotope signatures of DIC were modeled using the concept of open- and closed-system conditions with respect to dissolution of carbonate phase in the unsaturated zone. The parameters adopted for calculating the chemical and isotope characteristics of the DIC reservoir under open- and closed-system conditions are summarized in Table 2.

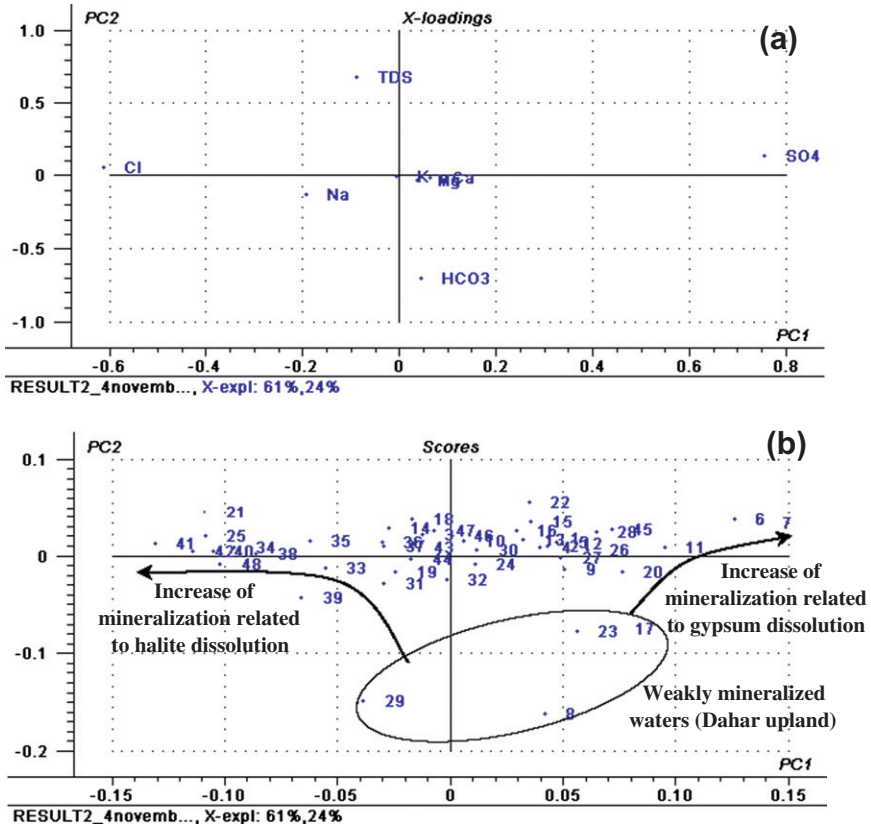

Fig. 4. Principal component analysis of Turonian groundwater.

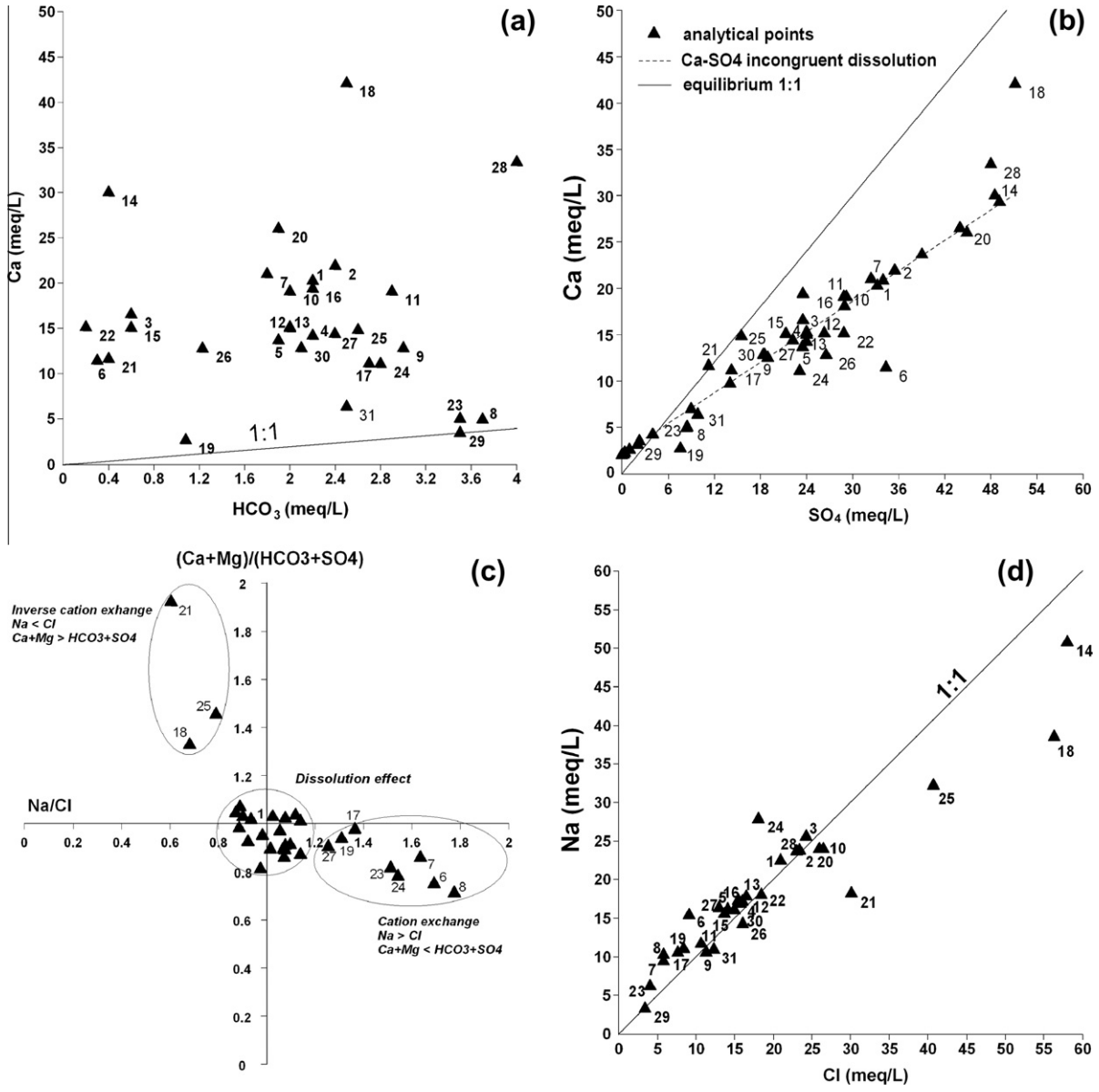

Fig. 5. Relationships between major elements in the analyzed groundwater samples: (a) Ca vs. HCO_3, (b) Ca vs. SO_4 (dashed line indicates proportions between Ca and SO_4 during incongruent dissolution of dolomite and gypsum), (c) [(Ca + Mg)/(HCO_3 + SO_4)] vs. [Na/Cl], and (d) Na vs. Cl.

The modeled isotopic evolution of theDIC pool under closed- and open-system conditions is shown in Fig. 9. It is apparent that under open-system conditions the $\delta^{13}C$ of the DIC reservoir evolves towards values equal to ca. −14‰ while the radiocarbon content is buffered at 100 pmc, the value assumed for the soil CO_2 reservoir. On the other hand, under closed-system conditions both $\delta^{13}C$ and the radiocarbon content of DIC are gradually reduced, approaching the values of ca. −10‰ and around 50 pmc, respectively, depending on the assumed initial conditions, mainly partial pressure of soil CO_2 and its ^{13}C content. It is apparent from the data presented in Fig. 9 that the calculated DIC contents under closed-system conditions are substantially lower than the measured values. In contrast, under open-system conditions the calculated DIC content is within the range of the measured values but the calculated C isotope composition of the DIC reservoir is far off the measured values. Although it would be possible in this case to explain generally lower ^{14}C contents observed in the analyzed samples by the aging effect, this is not the case for the measured $\delta^{13}C$ values which are significantly higher that those generated by the open-system model. In order to reconcile the measured and calculated C isotope characteristics of the DIC pool, additional sources of C have to be postulated. It is apparent from the discussion in Section 4.1 that geogenic CO_2 and incongruent dissolution of dolomite are the most probable additional sources of C in the studied systems.

The impact of geogenic CO_2 on isotope characteristics of the DIC reservoir has been modeled assuming that CO_2 with isotope characteristics typical for mantle CO_2 (no radiocarbon, $\delta^{13}C$ equal to ca. −5‰, Hoefs, 1980) is added to the solution until saturation conditions with respect to calcite are reached. It is apparent from Fig. 9 that admixture of CO_2 of mantle origin leads to chemical and isotope characteristics of the DIC pool which are in broad agreement with the measured values. However, the fact that a number of data points in Fig. 10a reveals higher ^{14}C concentrations than the modeled ones for the closed-system model, suggests that in reality the conditions in recharge area(s) are somewhere in-between open- and closed-system conditions with respect to soil CO_2.

The process of incongruent dissolution of dolomite and gypsum with simultaneous precipitation of calcite has a large potential for

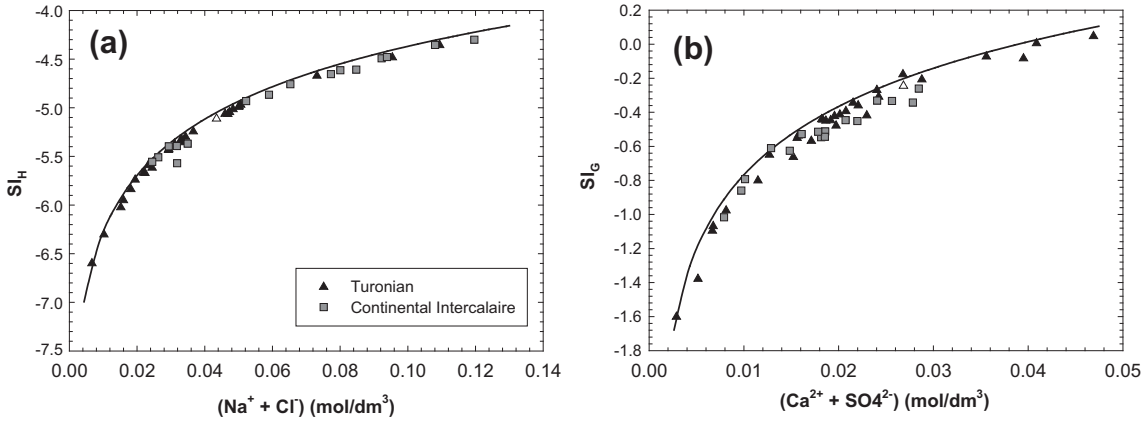

Fig. 6. Relationships between saturation indices and major elements in the analyzed groundwater samples: (a) halite: SI_H vs. (Na + Cl), (b) gypsum: SI_G vs. (Ca + SO_4). Solid lines represent theoretical relationship calculated with the PHREEQC-2 code.

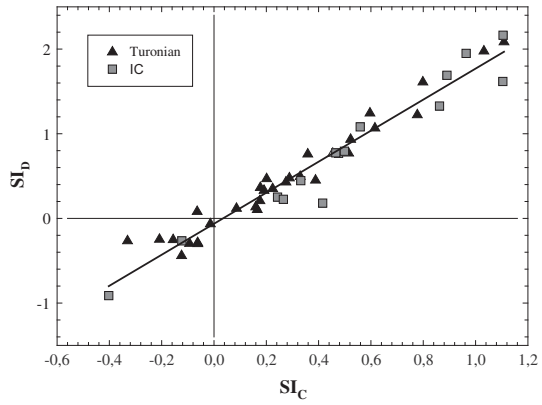

Fig. 7. The relationship between saturation indices with respect to calcite (SI_C) and dolomite (SI_D) for analyzed Turonian and Continental Intercalaire groundwater samples. Solid line represents linear fit to the analytical data.

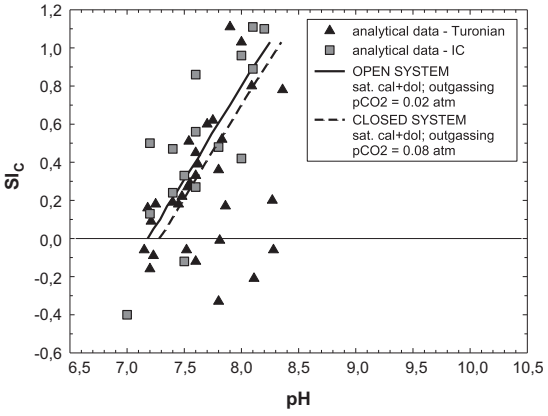

Fig. 8. Evolution of calculated and measured values of the saturation index (SI_C) as a function of pH in the analyzed groundwater samples, resulting from outgassing of CO_2. Both open- and closed-system conditions during formation of DIC reservoir in the solution were considered in the calculations (see text for details).

substantial modification of the C isotope signature of the DIC pool formed in the recharge area. For instance, while saturation in calcite at 25 °C and pCO_2 = 0.01 atm (open-system conditions) requires ca. 1.6 mmol of this mineral to be dissolved in the solution, saturation with respect to dolomite and gypsum achieved under closed-system conditions would require further dissolution

Table 2
Parameters adopted for calculating chemical and isotope characteristics of the DIC reservoir. Two values of CO_2 partial pressure in the soil were considered: 0.01 and 0.005 atm.

Parameter	Open system	Closed system
Initial parameters		
Partial pressure of soil CO_2 (atm)	0.01 (0.005)	0.01 (0.005)
Temperature in the soil (°C)	25	25
Isotopic composition of soil CO_2	−20‰; 100 pmc	−20‰; 100 pmc
Isotopic composition of carbonate phase	0‰; 0 pmc	0‰; 0 pmc
Parameters of DIC pool at equilibrium		
TDIC content (mmol/L)	3.56 (2.69)	0.71 (0.39)
$\delta^{13}C$ of TDIC (‰)	−12.9 (−12.6)	−10.2 (−9.5)
Radiocarbon content of TDIC (pmc)	100 (100)	49.4 (46.2)
Parameters of CO_2 added to the system		
$\delta^{13}C$ (‰)	−5‰	−5‰
Radiocarbon content (pmc)	0	0

of 11.3 mmol of dolomite and 24.6 mmol of gypsum, with simultaneous precipitation of ca. 22.9 mmol of calcite. Dolomite does not contain radiocarbon and its $\delta^{13}C$ value should be enriched by approximately 2.6‰ with respect to calcite (Deines et al., 1974; Ohmoto and Rye, 1979). Consequently, dissolution of dolomite will lead to gradual reduction of ^{14}C content and increase of $\delta^{13}C$ values of the DIC reservoir. The evolution of $^{14}C/^{12}C$ and $^{13}C/^{12}C$ ratios as a function of DIC during incongruent dissolution of dolomite has not been modeled. However, one may expect that the corresponding trajectories in Fig. 9a and b would be similar to those representing addition of geogenic CO_2 to the solution under closed-system conditions.

It is worth noting that in the case of incongruent dissolution of dolomite one may expect some relationship between $\delta^{13}C$ values of the DIC reservoir and $SO_4^{=}$ content in the solution, which can be considered as an indicator of the extent of dedolomitization reactions. Indeed, such a relationship has been observed in the analyzed groundwater samples, particularly for the Turonian aquifer system (Fig. 10). Interestingly, two wells (Nos. 43 and 46) which in Table 1 represent the CI aquifer, appear on Fig. 10 as distinct outliers, suggesting that they are more representative of the Turonian system. In fact, the high position of the screens in those two wells points to a Turonian origin of sample 43 and 46.

Outgassing of CO_2 which is responsible for the observed supersaturation in calcite and dolomite of the studied groundwaters should lead to an increase of $\delta^{13}C$ of C remaining in the solution.

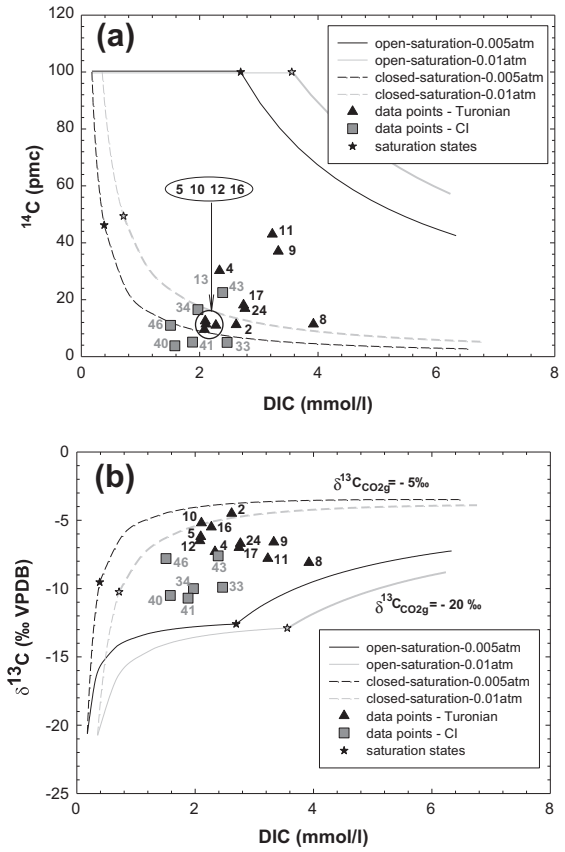

Fig. 9. Carbon isotope evolution of DIC reservoir under open- and closed-system conditions. Stars indicate saturation of the solution with respect to $CaCO_3$. Subsequent evolution of the DIC reservoir (grey lines), resulting from input of additional carbon, was calculated via consecutive equilibrium stages with a solid carbonate phase (see text for details).

However, this increase will be partly compensated by fractionation occurring during precipitation of calcite. Modeling suggests that the resulting shift of $\delta^{13}C$ values is in the order of 1‰.

Finally, it has to be kept in mind that the modeling approach outlined above does not account for mixing of different water types with respect to chemical and isotope characteristics of the DIC reservoir. Such mixing is suggested by the stable isotope composition of water (cf. Section 4.3).

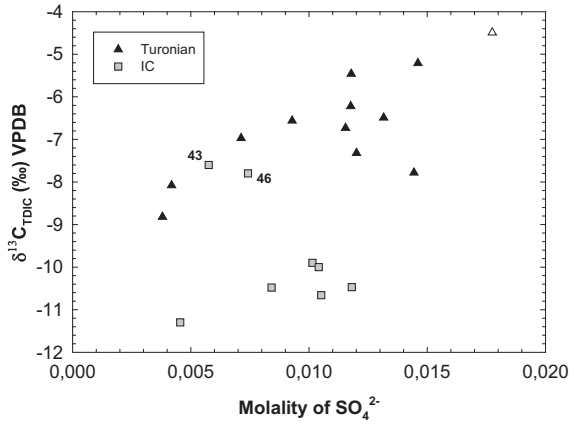

Fig. 10. The relationship between $\delta^{13}C$ values of DIC reservoir and the SO_4^{2-} content of the analyzed groundwater samples.

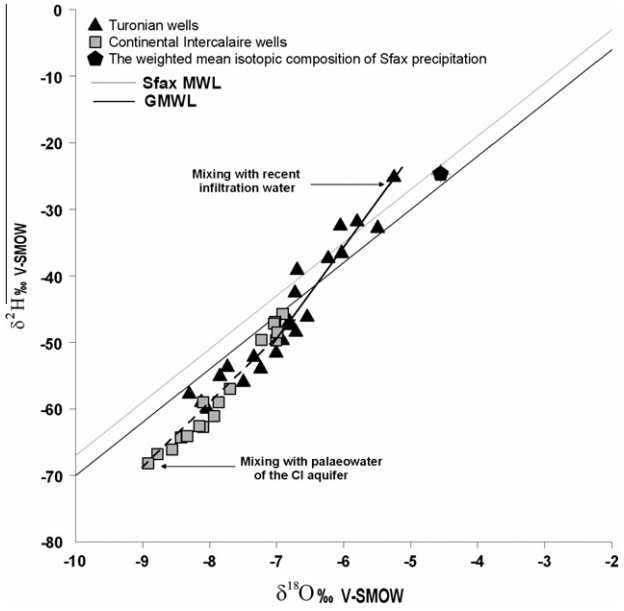

Fig. 11. Stable isotope composition of groundwater from the Turonian and Continental Intercalaire aquifers.

4.3. Deuterium and oxygen-18

The stable isotope composition of Turonian groundwater samples varies over a relatively wide range, from −8.3 to −5.3‰ for $\delta^{18}O$ and from −60 to −25‰ for δ^2H (Table 1). The corresponding ranges of δ values for the Continental Intercalaire samples are from −8.9‰ to −6.9‰ for $\delta^{18}O$ and from −68.2‰ to −45.7‰ for δ^2H.

The available stable isotope data are presented in Fig. 11 in the δ^2H–$\delta^{18}O$ space. The Regional Meteoric Water Line (RMWL) and the Global Meteoric Water Line (GMWL) are shown for comparison. The RMWL was calculated for the 13-a record of monthly precipitation collected at Sfax meteorological station (cf. Fig. 1) and is defined by the equation: $\delta^2H = 8\delta^{18}O + 13‰$ (Abid et al., 2009). The long-term weighted mean isotopic composition of Sfax precipitation is −4.6 ‰ and −25‰, for $\delta^{18}O$ and δ^2H, respectively. It is expected that the mean stable isotope signature of local rainfall in the recharge areas of the Turonian aquifer (Dahar uplands in the south and Chotts in the north) will be depleted in heavy isotopes with respect to Sfax rainfall due to their higher elevation and inland location.

The stable isotope data presented in Fig. 11 reveal two major trends reflecting regional mixing between different water types. The first trend line plots almost parallel to the GMWL and is shifted to the right-hand side of it. It extends from ca. −8.8‰ in $\delta^{18}O$ (isotopically most depleted CI waters) to approximately −7‰. The position of the trend line is typical for old paleowaters occurring in the northern part of Africa. The observed isotopic composition of CI waters agrees well with the values obtained in previous studies in Southern Tunisia by Gonfiantini et al. (1974), Fontes et al. (1983), Edmunds et al. (2003) and Zouari et al. (2003). This characteristic shift in stable isotope composition, when compared to modern infiltration waters reflects changes in the isotopic signature of regional rainfall during the late Pleistocene and early Holocene. Significant ages of these waters are confirmed by low radiocarbon content. The majority of Turonian waters revealing the isotopic signature typical for old groundwaters are located in the El Hamma hydraulic sill zone, where differences in hydraulic heads allow an upward leakage of the CI waters towards the Turonian aquifer.

The second trend line cuts the GMWL and RMWL lines and extends from ca. −7.0‰ in $\delta^{18}O$ to approximately −5.5‰. It most

probably reflects regional mixing between Turonian waters and the recent infiltration water. The presence of a fresh component is confirmed by significant ^{3}H content measured in some wells (1.3 TU in well No. 11; 2.4 TU in well No. 27). Waters of this group are not affected by evaporation and are characterized by relatively high ^{14}C concentration (30–43 pmc). They originate from wells located in the vicinity of Miocene and Cretaceous outcrops.

The mixing proportions inferred from stable isotope mass balance (Trabelsi et al., 2009; Abid, 2010) prove that the contribution of the CI system to the recharge of the Turonian aquifer is very significant and may reach 100% in some areas, such as the El Hamma region.

5. Conclusions

Combined use of hydrochemistry and isotopic composition of groundwater samples collected in two regional aquifers in southern Tunisia allowed a more detailed insight into the processes controlling chemical composition of groundwater and wide-scale interaction of these two aquifer systems.

Analysis of the dissolved constituents revealed that two major processes control the observed chemical composition: (i) incongruent dissolution of carbonate minerals (calcite, dolomite) coupled with dissolution of gypsum and precipitation of calcite, and (ii) cation exchange reactions. Further, it has been demonstrated that dissolution alone cannot account for the observed high supersaturation states of groundwater with respect to calcite and dolomite. The observed supersaturation can be generated only if significant outgassing of the solution, which is formed under relatively high partial pressure of CO_2, occurs in the system. Such high partial pressures of CO_2 can be induced by geogenic CO_2 which enters water-bearing horizons of the CT and CI aquifers via deep tectonic faults and discontinuities. Significant outgassing of the collected groundwater samples is confirmed by precipitation of calcite occurring in a number of exploited wells.

The presence of geogenic CO_2 in the investigated region was further supported by C isotope data of the DIC reservoir. An additional source of C with the isotope characteristics typical for mantle CO_2 ($\delta 13C \approx -5‰$, lack of radiocarbon) may explain, apart from the dedolomitization process, the observed range of $^{13}C/^{12}C$ and $^{14}C/^{12}C$ ratios in the DIC pool of the analyzed groundwater samples.

The stable isotope composition of groundwater samples representing CT and CI aquifers provide strong evidence for regional interaction between both systems. It is clear from the available data that upward seepage from the Continental Intercalaire aquifer, favored by deep faults, constitutes an important recharge mechanism for the Turonian aquifer, in addition to present-day recharge.

The relatively low radiocarbon content of groundwater samples analyzed in the framework of this study, as well as radiocarbon data obtained in other studies which have been carried out in the region in the past decades (e.g. Guendouz et al., 1997; Edmunds et al., 2003; Abid, 2010), coupled with distinct stable isotope signature of these waters, suggest a significant age of groundwater in those systems, extending from Late Pleistocene to late Holocene. Although radiocarbon ages in excess of 25–30 ka BP have been calculated and reported by various authors for groundwater exploited in southern Tunisia, they have to be treated with caution in view of complex C chemistry, which involves inconguent dissolution of dolomite and gypsum and/or presence of geogenic CO_2 of mantle origin, supplemented by large-scale regional mixing of water between different aquifer systems present in the area.

As Tunisia suffers from limited surface water resources, particularly in its southern part, sustainable management of available groundwater resources is a critical factor in further economic development of the country. The integrated approach towards better understanding of the quality and dynamics of groundwater presented here may constitute a valuable tool for managers to design appropriate strategies for exploitation of this national precious resource.

Acknowledgements

We wish to thank the Laboratory of the International Agency of Atomic Energy (IAEA) and the Laboratory of Radio-Analyses and Environment of the National Engineering School of Sfax (ENIS) for the chemical and isotopic analysis. Special thanks are directed to the staff members of Gabes, Kebili, Tataouine and Medenine Water Resources Division/Agriculture Ministry. The comments of Associate Editor Prof. Mike Edmunds and two anonymous reviewers helped to improve the manuscript significantly. The contribution of M.D. and K.R. was supported by the statutory funds of AGH University of Science and Technology, Krakow, Poland (Project No. 11.11.220.01).

References

Abid, K., 2010. Identification et caractérisation hydrogéologique et géochimique de la nappe du Continental Turonien dans le Sud tunisien et sa reltion avec les aquifères adjacents. Thèse de Doctorat, Ecole Nationale d'Ingénieurs de Sfax, Tunisie.

Abid, K., Trabelsi, R., Zouari, K., Abidi, B., 2009. Caractérisation hydrogéochimique de la nappe du Continental Intercalaire (Sud tunisien). Hydrolog.l Sci.-J.-des Sci. Hydrologiques 54, 526–537.

Abid, K., Zouari, K., Dulinski, M., Chkir, N., Abidi, B., 2011. Hydrologic and geologic factors controlling groundwater geochemistry in the Turonian aquifer (southern Tunisia). Hydrogeol. J. 19, 415–427.

Abidi, B., Ben Baccar, B., 2001. La nappe du Continental Intercalaire du sud-est Tunisien: analyse de la situation actuelle. Direction Générale des Ressources en Eau.

Boltenhagen, C., 1981. Paléogéographie du Crétacé moyen de la Tunisie centrale. Actes 1er Cong. Nat. Sci. Terre., Fac. Sc., Tunis, Tunisia, 97–114.

Bouaziz, S., 1995. Etude de la tectonique cassante dans la plateforme et l'Atlas Sahariens (Tunisie Meridionale): évolution des paleochamps de contraintes et implications géodynamiques. Thèse de Doctorat, Fac. Sci. de Tunis, Tunisie.

Bouaziz, S., Barrier, E., Soussi, M., Turki, M.M., Zouari, H., 2002. Tectonic evolution of the northern African margin in Tunisia from paleostress data and sedimentary record. Tectonophysics 357, 227–253.

Busson, G., 1967. Le Mésozoïque saharien, première partie: l'Extrême-Sud Tunisien. Centre National de Recherche Scientifique (CNRS), Zones arides, Série Géologie 8.

Castany, G., 1954. L'accident sud tunisien et ses relations avec l'accident sud-atlasique. C.R. Acad. Sci., Paris, 238.

Clark, I.D., Fritz, P., 1997. Environmental Isotopes in Hydrogeology. Lewis Publishers.

Coleman, M.L., Shepherd, T.J., Durham, J.J., Rouse, J.E., Moore, G.R., 1982. Reduction of water with zinc for hydrogen isotope analysis. Anal. Chem. 54, 993–995.

Coplen, T.B., 1996. New guidelines for reporting stable hydrogen, carbon, and oxygen isotope-ratio data. Geochim. Cosmochim. Acta 60, 3359–3360.

Deines, P., Langmuir, D., Harmon, R.S., 1974. Stable carbon isotope ratios and the existence of a gas phase in the evolution of carbonate ground waters. Geochim. Cosmochim. Acta 38, 1147–1164.

Drever, J.I., 1988. The Geochemistry of Natural Waters. Prentice Hall, Englewood Cliffs.

Edmunds, W.M., Shand, P., Guendouz, A.H., Moulla, A.S., Mamou, A., Zouari, K., 1997. Recharge Characteristics and Groundwater Quality of the Grand Erg Oriental Basin. British Geological Survey, London, UK.

Edmunds, W.M., Guendouz, A., Mamou, A., Moulla, A., Shand, P., Zouari, K., 2003. Groundwater evolution in the Continental Intercalaire aquifer of southern Algeria and Tunisia: trace element and isotopic indicators. Appl. Geochem. 18, 805–822.

Ellouze, N., 1984. Etude de la subsidence de la Tunisie atlasique orientale et de la Mer pélagienne. Thèse 3ème cycle, Univ. Paris VI.

Epstein, S., Mayeda, T.K., 1953. Variations of 180 content of waters from natural sources. Geochim. Cosmochim. Acta 4, 213–224.

ERESS, 1972. Etude des Ressources en Eau de Sahara Septentrional. UNESCO, Paris (7 Vols. and Annexes).

Esbensen, K.H., 2002. Multivariate Data Analysis – In Practice, fifth ed. Camo Process, Oslo.

Fontes, J.C., Coque, R., Dever, L., Filly, A., Mamou, A., 1983. Paléohydrologie isotopique de l'wadi el Akarit (sud tunisien) au Pléistocène et à l'Holocène. Palaeogeog. Palaeontol. Palaeogeol. 43, 41–61.

Freeze, R.A., Cherry, J.A., 1979. Groundwater. Prentice Hall, Englewood Cliffs, NJ.

Gabtni, H., Jallouli, C., Mickus, K.L., Zouari, H., Turki, M.M., 2009. Deep structure and crustal configuration of the Jeffara basin (Southern Tunisia) based on regional gravity, seismic reflection and borehole data: how to explain a gravity maximum within a large sedimentary basin? J. Geodynam. 47, 142–152.

Gonfiantini, R., Conrad, G., Fontes, J.-C.H., Sauzay, G., Payne, B.R., 1974. Etude isotopique de la nappe du CI et ses relations avec les autres nappes du Sahara Septentrional. In: Proc. Symp. Isotope Hydrology, Vienna. IAEA, Vienna, pp. 227–241 (March).

Guendouz, A., Moulla, A.S., Edmunds, W.M., Shand, P., Poole, J., Zouari, K., Mamou, A., 1997. Palaeoclimatic information contained in groundwaters of the Grand Erg Oriental, N. Africa. In: Isotope Techniques in the Study of Past and Current Environmental Changes in the Hydrosphere and Atmosphere. IAEA, Vienna, pp. 555–571.

Haynes, C.V., Haas, H., 1980. Radiocarbon evidence for Holocene recharge of groundwater, Western Desert, Egypt. Radiocarbon 22, 705–717.

Hoefs, J., 1980. Stable Isotope Geochemistry. Springer-Verlag, Berlin; Heidelberg, New York, pp. 86–87.

Kamel, S., 2007. Caractérisation hydrodynamique et géochimique des aquifères du Djérid (Sud-Ouest tunisien). Thèse de 3ème cycle, Faculté Sciences de Tunis.

Mamou, A., 1990. Caractéristiques, Evaluation, Gestion des Ressources en eau du Sud Tunisien. Thèse de Doctorat, Es Science, Univ., Paris Sud.

Ohmoto, H., Rye, R.O., 1979. Isotopes of sulfur and carbon. In: Barnes, H.L. (Ed.), Geochemistry of Hydrothermal Ore Deposits. John Wiley & Sons, pp. 509–561.

Observatoire Sahara et Sahel (OSS), 2003. Système aquifère du Sahara septentrional: gestion commune d'un bassin transfrontière. Rapport de synthèse, OSS, Tunisie.

Parkhurst, D.L., Appelo, C.A.J., 1999. User's Guide to PHREEQC (Version 2) – A Computer Program for Speciation, Batch-Reaction, One-Dimensional Transport, and Inverse Geochemical Calculations. US Geol. Surv. Water-Resour. Invest. Rep. 99-4259, USGS.

Stuiver, M., Polach, H., 1977. Reporting of ^{14}C data. Radiocarbon 19, 355–363.

Trabelsi, R., Kacem, A., Zouari, K., Rozanski, K., 2009. Quantifying regional groundwater flow between Continental Intercalaire and Djeffara aquifers in Southern Tunisia using isotope methods. Environ. Geol. 58, 171–183.

Zouari, K., Chkir, N., Ouda, B., 2003. Palaeoclimatic Variation in Maknassi Basin (Central Tunisia) During Holocene Period Using Pluridisplinary Approaches. IAEA Tech. Report 80-88. International Atomic Energy Agency, Vienna, Austria.